

Controlled formation of metallic nanowires via Au nanoparticle ac trapping

L Bernard, M Calame, S J van der Molen, J Liao and C Schönenberger

Institute of Physics, University of Basel, CH-4056 Basel, Switzerland

E-mail: michel.calame@unibas.ch

Received 16 January 2007, in final form 15 April 2007

Published 8 May 2007

Online at stacks.iop.org/Nano/18/235202

Abstract

Applying ac voltages, we trapped gold nanoparticles between micro-fabricated electrodes under well-defined conditions. We demonstrate that the nanoparticles can be controllably fused together to form homogeneous gold nanowires with pre-defined diameters and conductance values. Whereas electromigration is known to form a gap when a dc voltage is applied, this ac technique achieves the opposite, thereby completing the toolkit for the fabrication of nanoscale junctions.

1. Introduction

Novel nanometre-scale electronic systems have been extensively developed during the last few years. For example, field-effect transistors made from carbon nanotubes [1] and organic molecules [2, 3] are being designed to constitute alternative routes to Si-based technology. Molecular electronics in particular combines several advantages: nanometre-scale size, flexibility of chemical synthesis and discrete energy levels. These aspects make molecules appear as promising building blocks for ultimate nano-electronics [4]. However, a key challenge within this size range remains the control of the connection between a few molecules and macroscopic current and voltage leads [5]. This requires the fabrication of contacts down to the size of a few nanometres. Electron-beam lithography can presently only hardly reach sub-10 nm resolution, or under very specific conditions [6–8]. Thus, new techniques need to be developed to produce nanoscale contacts. Among others, one philosophy is to start from e-beam prefabricated micro-electrodes and decrease the gap in a second step, for example via electrodeposition [9]. A promising method is to close the gap by metallic nanoparticles, used as intermediates, linking the molecules to the electrodes [10–14]. Hence, there is a need for the precise positioning of nanoparticles within larger structures.

A simple and controllable method to position nanoparticles is reported here. It consists of aligning and contacting colloids by means of dielectrophoresis (ac trapping) [15–17]. This technique has previously been used to manipulate a variety of micrometre- and nanometre-size objects including biopolymers [18, 19], cells [20] and metallic colloids

[21–23, 10, 24, 25]. However, a systematic approach is still lacking. This is true in particular concerning the assembly of metallic particles in sub-micrometre gap sizes. In the present work, the process of ac trapping nanoparticles with diameters in between 10 and 100 nm into gaps of widths ranging from 20 to 500 nm has been investigated. Remarkably, the technique enables one to form continuous nanowires of tunable diameter between microfabricated electrodes. This process can be initiated by choosing the proper ac voltage and series impedance.

2. Experimental details

Pairs of planar, tip-shaped gold (Au) electrodes facing each other were patterned on a Si/SiO₂ substrate using conventional UV and electron-beam lithography (EBL). Before each fabrication step, the substrate was cleaned in acetone, followed by isopropanol and was finally exposed to an oxygen plasma for 5 min. After resist spinning, exposure and development, a 5 nm thick adhesion layer of Ti was deposited prior to the evaporation of a 35 nm Au layer. The tips of the electrodes pairs were separated by a gap typically ranging between 20 and 100 nm. Using an angle evaporation technique, the gap size can be reduced to less than 20 nm, however, with a relatively small yield (~5%).

Colloidal solutions of charge-stabilized Au particles were prepared following the method of Turkevich *et al* [26]. A 0.5 mM solution of HAuCl₄ was reduced with aqueous citric acid at boiling temperature. This resulted in nearly monodisperse charge-stabilized Au colloids with a diameter

between 10 and 30 nm, depending on the reducing agent concentration. Using these charge-stabilized Au colloids as the starting material, we have also prepared alkane-thiol encapsulated Au colloids following the method of Huang *et al* [27]. For subsequent experiments, the encapsulated colloidal particles were dissolved in a 1:1 mixture of hexane and dichloromethane.

Trapping of the Au nanoparticles was performed via dielectrophoresis (DEP) by applying an ac electric field \vec{E} between the two electrodes. The dielectrophoretic force \vec{F}_{DEP} acting on a homogeneous, isotropic particle of radius a is proportional to the gradient of the electric field amplitude squared and is [17]:

$$\vec{F}_{\text{DEP}} = \pi a^3 \epsilon_m \cdot \text{Re} \left[\frac{\tilde{\epsilon}_p - \epsilon_m}{\tilde{\epsilon}_p + 2\epsilon_m} \right] \cdot \nabla |\vec{E}|^2$$

where Re denotes the real part. The effective polarizability of the particle in the medium is expressed by the relative permittivities of the particle $\tilde{\epsilon}_p$ and the medium ϵ_m . This force typically ranges from 0.1 to 1 pN [16, 17].

A circuit diagram of our set-up is sketched in figure 1. The scheme includes a series capacitor C_s and a series resistor R_s , which constitute a total series impedance Z_s . The capacitor was placed in the circuit to filter out any dc component and to avoid electrochemical processes or electromigration [28]. It also prevented further effects due to, for instance, the electrophoretic mobility of the ionic solution, which can influence the motion of the suspended nanoparticles. To measure the time dependence of the current, $i(t)$, we recorded the voltage drop over R_s . For this, both a time-averaging lock-in amplifier and a fast digital oscilloscope were used. The lock-in amplifier continuously monitored the trapping process with a time resolution of ≈ 100 ms. In contrast, the oscilloscope, which provided a much faster time resolution of ≈ 100 ns, was adjusted to trigger at the trapping event when a significant increase of the current amplitude \hat{I} was monitored. In this way we measured the delay time until a particle is trapped and the temporal evolution of the impedance during junction formation. In order to limit the number of parameters in the process, we fixed the frequency f of the ac field throughout the trapping experiments to a value of 1 MHz. This allowed the manipulation of nanoparticles with diameters ranging between 10 and 100 nm at concentrations of the order of 10^{13} ml^{-1} . Typical values for the total input voltage V_{in} and the series resistor R_s were $V_{\text{in}} \leq 3.5 \text{ V}$ and $0 \Omega \leq R_s \leq 500 \Omega$, respectively. Throughout this paper, the symbols I , V , R and P refer to the RMS values of the current, voltage, resistance and dissipation at (in) the junction, respectively. During the trapping process, they are time-dependent. Their final values, once the trapping is completed, are denoted by I_f , V_f , R_f and P_f , respectively.

3. Results and discussion

We explored various types of colloids with a main focus on charge-stabilized Au colloids with a diameter of $25 \pm 5 \text{ nm}$. To investigate the trapping process in detail, the current through 103 junctions was measured during and after the trapping of these specific particles. All samples were prepared following the same procedure. Figure 2(A) shows a typical lock-in

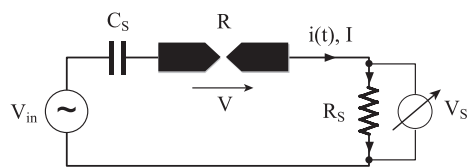


Figure 1. Schematics of the trapping circuit. Both an oscilloscope and a lock-in amplifier record the voltage drop V_s over the series resistor R_s . Together, R_s and the series capacitor $C_s = 1.5 \text{ nF}$ form the total series impedance Z_s .

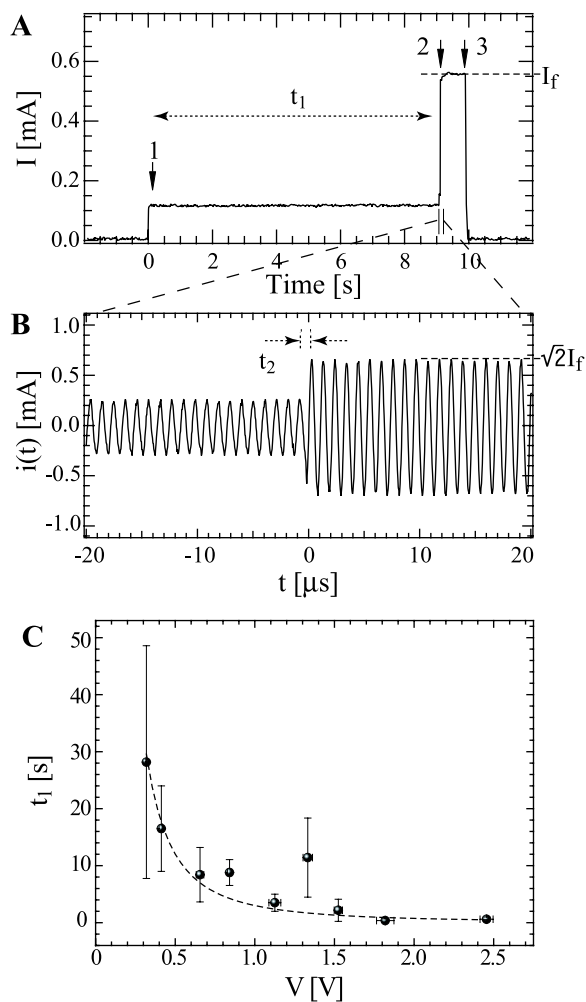


Figure 2. (A) Typical record of the rms current I through the junction during both trapping and anchoring processes, with $V_{\text{in}} = 1 \text{ V}$ and series impedance $|Z_s| = 467 \Omega$. Arrows 1, 2 and 3 mark the time when the voltage was applied, the contact was made and the voltage was set to 0, respectively. The characteristic time for trapping, t_1 , is defined as the time between arrows 1 and 2. (B) Close-up view of the ac current $i(t)$ measured with an oscilloscope around the contacting event ($t = 0$). (C) t_1 as a function of the voltage over the junction V (at $t < t_1$). Each point is an average over several data points; the error bars correspond to the standard error. The dotted line represents a $1/V^2$ dependence.

measurement of the current I flowing through a junction during trapping. First, a colloidal solution droplet was deposited on the device ($t < 0$). Next, an ac trapping voltage V_{in} was applied at $t = 0$ to attract the nanoparticles to the junction. This

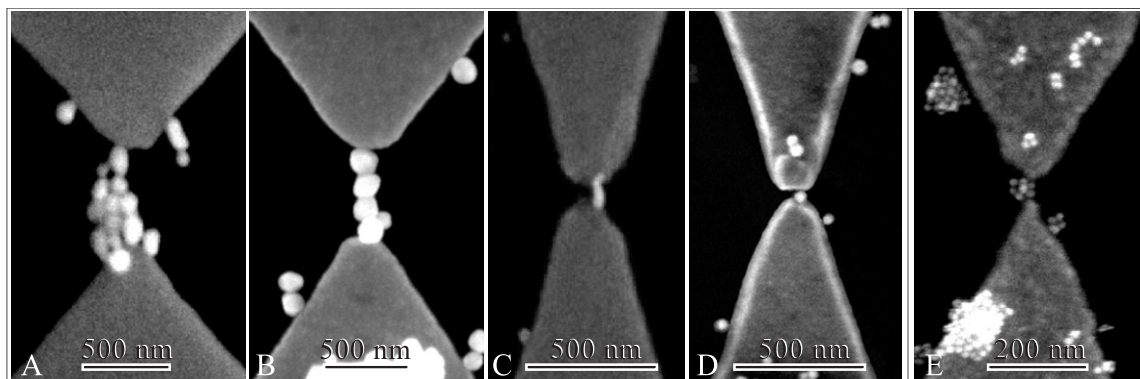


Figure 3. Scanning electron micrographs of junctions prepared under various conditions. (A) Large gap (500 nm) with large nanoparticles (120 ± 20 nm): parameters $V_{in} = 2$ V, $|Z_s| = 111 \Omega$; final resistance $R_f = 280 \Omega$. (B) Large gap (560 nm) with large nanoparticles (120 ± 20 nm): $V_{in} = 1$ V, $|Z_s| = 111 \Omega$; $R_f = 50 \Omega$. (C) Small gap (40 nm) with a wire formed by small nanoparticles (25 ± 5 nm): $V_{in} = 1$ V, $|Z_s| = 148 \Omega$; $R_f = 160 \Omega$. (D) Small gap (30 nm) with a single small nanoparticle (25 ± 5 nm): $V_{in} = 1.8$ V, $|Z_s| = 467 \Omega$; $R_f = 4.8$ M Ω . (E) Small gap (20 nm) with small C_{12} -functionalized nanoparticles (10 ± 1 nm): $V_{in} = 1$ V, $|Z_s| = 147 \Omega$; $R_f = 4$ M Ω .

gave rise to a detectable leakage current through the solution (arrow 1). After the duration t_1 of typically a few seconds to 1 min, a large current increase was suddenly observed (arrow 2). This event signals the formation of a conducting bridge within the gap due to the trapping of individual nanoparticles. The conductance jump takes place when the last nanoparticle gets trapped and completes the closing of the gap. After this increase, the current remained constant and, finally, the input voltage V_{in} was set to zero (arrow 3). We note that in a few particular cases the current did not increase in a single step, but rather displayed multiple steps, suggesting the formation of a few conducting bridges in parallel. Figure 2(B) shows a typical oscilloscope trace of $i(t)$, set up to trigger exactly at the current increase (arrow 2, figure 2(A)). We see that the junction changes its resistance typically within $t_2 \sim 1 \mu\text{s}$. Figure 2(C) shows the dependence of the average trapping time t_1 on the voltage over the junction V (for $t < t_1$). The trapping time roughly scales with the inverse of the voltage squared $1/V^2$, which agrees with the expectation for a driven particle movement impeded by viscous friction. In that case the velocity scales with the driving force which is, according to the expression for the dielectrophoretic force, proportional to the electric field squared, and hence to the voltage squared.

After each trapping experiment, scanning electron microscopy (SEM) inspection of the samples revealed that in 67 cases the junctions showed no sign of breakdown. Figure 3 reports a set of representative results. First, we focus on figures 3(A) and (B). Here, nanoparticles with a relatively large diameter of 120 ± 20 nm were trapped into ~ 500 nm large gaps. The trapping conditions for both cases were identical, except for the applied voltage V_{in} : 2 V in case (A) and 1 V in case (B). We clearly observe a larger number of trapped particles in (A) than in (B). This illustrates that one can tune the number of nanoparticles bridging the gap by adjusting the trapping voltage. The electric field required for optimal trapping amounts to about $E \approx 10^7$ V m $^{-1}$. In figure 3(B), a well-ordered chain of nanoparticles was formed with a junction resistance of *only* 50 Ω . This is surprising and indicates that, after the nanoparticles were trapped, a second, ‘anchoring’, process took place. During anchoring, the colloids become physically and electrically connected,

leading to a low final resistance. Figure 3(C) shows a device in which even smaller particles, i.e. 25 ± 5 nm, were trapped, with an applied voltage $V_{in} = 1$ V. Remarkably, the individual colloids are not distinguishable any longer. Instead of building a chain, as in figure 3(B), the particles have fused together forming a *wire* with a well defined diameter. The final resistance of this wire is comparatively low, i.e. 160 Ω . Figure 3 shows that the anchoring process can lead to the formation of two distinct structures: chains or wires. Below, we will discuss this phenomenon in more detail. Finally, in figures 3(D) and (E), we show examples of junctions with relatively large final resistances in the megaohm range. In figure 3(D), a single nanoparticle (25 ± 5 nm) was trapped. In contrast to figures 3(A)–(D) where charge-stabilized colloids were used, figure 3(E) shows a typical result for the trapping of dodecanethiol ($C_{12}H_{25}S$)-functionalized nanoparticles of 10 nm diameter within a 30 nm gap. Unlike the former cases, devices made with functionalized particles never displayed fusing and the resistance values were always large ($>M\Omega$).

In 11 cases of the 67 successful trapping experiments with 25 ± 5 nm diameter charge-stabilized nanoparticles, the final junction resistance R_f was much larger than 1 M Ω . This indicates that no metallic contact was established between the nanoparticles and the electrodes. An overview of the rest of the data set (56 experiments) is given in figure 4. Here, we plot the final device resistance R_f as a function of the current I_f , both measured at the end of the trapping and anchoring process. There is quite some scatter in the final resistance of the devices. Nevertheless, the data set is confined between a lower and an upper bound given by the voltage $V_f = I_f R_f$. More precisely, the voltage over the junction always lies in between 0.2 and 1.6 V, as indicated by the dotted lines, a typical value being 0.9 V. The lower bound in figure 4 is related to the trapping process: if the electric field is too small, trapping does not take place. In contrast, a voltage that is too large leads to sample destruction after trapping, as evidenced by ‘burnt’ electrodes which are modified on a macroscopic scale. This breakdown process is likely related to a thermal runaway by excessive Joule heating as reported in electromigration experiments on nanojunctions [29–31]. The open and solid data points in figure 4 relate to two different kinds of junctions. The solid

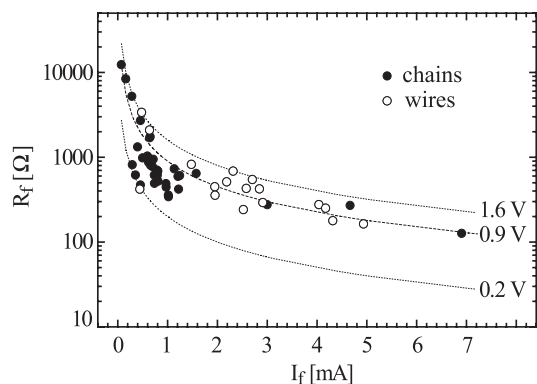


Figure 4. Final resistance R_f versus current I_f of the junctions showing successful trapping and anchoring (56 devices). The voltage over the junctions $V_f = I_f R_f$ is bound by 0.2 V from below (no trapping) and 1.6 V from above (breakdown after trapping), as indicated by dotted lines. A typical voltage is 0.9 V (dashed line). Solid dots: chain formation; open dots: wire formation (as extracted from SEM images).

dots refer to junctions in which the nanoparticles formed chains during the trapping process (cf figure 3(B)), whereas the open dots relate to wire formation (cf figure 3(C)). It appears that the two subsets group together in figure 4, despite the clear scatter. Hence, figure 4 forms a good basis to speculate about the possible processes behind anchoring, chain and wire formation, as well as device breakdown.

We first focus on the moment when a set of nanoparticles is being trapped in the junction at $t = t_1$. These particles experience a large electric field in the gap region $\sim 10^7$ V m $^{-1}$, which induces a dipole in each of them. Consequently, the dipole–dipole interaction between the particles becomes significant, tending to line up the particles in the junction. This explains the preference for the initial chain formation. At that point, the charge-stabilized particles are not yet interconnected, so that the whole voltage drops over the tiny gaps (≤ 1 nm) between the particles. This has two consequences. First, the electric field is much more localized than before chain formation. Hence, the range of the DEP force is decreased, leading to a much smaller trapping probability for left-over particles in the solution. In this way, DEP is self-limiting. Second, the field over the gaps between the individual colloids tend to become very high, $\geq 10^8$ V m $^{-1}$. At such fields, surface diffusion of Au atoms is enhanced in the direction of the gap and can lead to the formation of narrow Au bridges between the nanoparticles [32, 33]. If no connections are formed, a device will have a high final resistance ($\gg 1$ M Ω), as observed in 11 of our 71 junctions made with charge-stabilized particles. As mentioned above, junctions prepared with alkanethiol-covered particles *always* yielded high resistance values, suggesting that the alkanethiol shell protects the colloids against field-driven atomic migration. However, in most devices with charge-stabilized particles, the particles were interconnected and the resistance of the devices dropped dramatically. One may wonder what determines the final value R_f of these junctions. To address this point, we refer to figure 5(A), where a histogram of $\log(R_f/|Z_s|)$ is plotted. This graph describes the probability distribution of the ratio of R_f to the total series impedance $|Z_s|$. We find that R_f is typically of the same

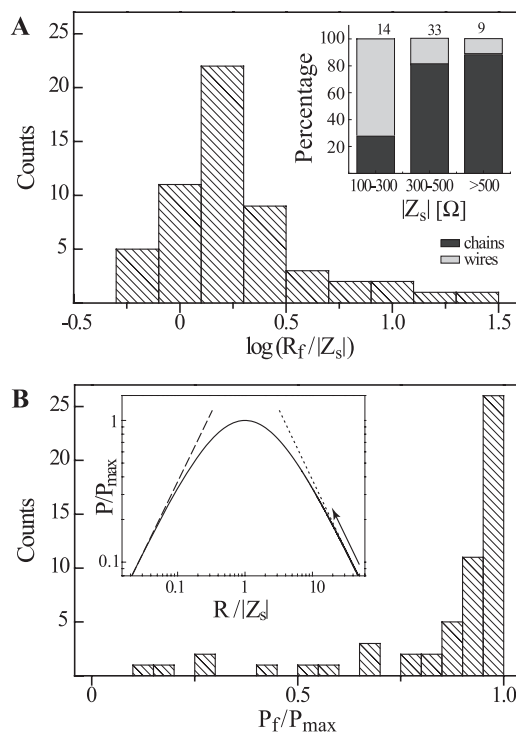


Figure 5. (A) Histogram of $\log(R_f/|Z_s|)$, for the data in figure 4. A single peak is seen with a maximum around $\log(R_f/|Z_s|) = 0.2$. The inset shows the percentage of chains (dark) and wires (light) for different values of $|Z_s|$. Wires are more favourably formed for lower $|Z_s|$. (B) Histogram of P_f/P_{\max} , where $P_f = V_f^2/R_f$. A clear majority of the devices have $P_f \approx P_{\max}$. The inset shows a calculation of P/P_{\max} as a function of $R/|Z_s|$, which reaches its maximum at $R = |Z_s|$ (calculation for $Z_s = 452 - 134i\Omega$). The arrow indicates that the resistance of our junctions decreases during homogenization. The dashed and dotted lines refer to the limiting cases of current- and voltage biasing, respectively.

order of magnitude as $|Z_s|$. The histogram features a clear peak with a maximum around a ratio of $\log(R_f/|Z_s|) = 0.2$, corresponding to $R_f = 1.6|Z_s|$. In the inset of figure 5(A), we show a stacked bar plot of the percentage of chains (dark) and wires (light) for three ranges of $|Z_s|$. Interestingly, chains are more common for higher $|Z_s|$, while wires are mostly found for lower $|Z_s|$. Figure 5(A) indicates that we can tune (at least roughly) the device properties via the series impedance.

To understand this, we bring forward a possible model of wire formation. We first note that a change in shape from chain to wire leads to a decrease of the total surface energy. Hence, we expect that surface tension is the effective driving force for the fusing process. Also, in order to transform a chain of spherical particles into a rod-like wire, a considerable diffusion of Au atoms is needed. Since diffusion is an activated process, an increase of the junction temperature by Joule heating will clearly facilitate wire formation. Before fusing, $R \gg |Z_s|$ and the junction is voltage-biased with the power P dissipated over the junction given by $P = V_{\text{in}}^2/R$. Once atomic diffusion sets in and the gaps start to fill up, the resistance decreases and consequently the dissipation increases. If the applied voltage V_{in} is too large, this can lead to a thermal runaway and sample breakdown. However, the series impedance Z_s also has an effect on P . It can self-limit the thermal runaway

process for moderate V_{in} . To see this, we note that the junction would be current-driven in the opposite regime $R \ll |Z_s|$. In that case, the local dissipation P is given by $P \approx RI^2$ and decreases with decreasing R , thus limiting the fusion process. The full dependence of P on $R/|Z_s|$ is shown in the inset of figure 5(B). There is a maximum power $P_{max} = V_{in}^2/4|Z_s|$ at $R = |Z_s|$. The dashed and dotted lines indicate the dissipation in the limiting cases of effectively current-biased and voltage-biased junctions, respectively. Based on this consideration, we expect the process to stop when $R \approx Z_s$ where the dissipation P reaches its maximum. Hence, the final dissipation P_f , measured at the end of successful junction formation, should be close to P_{max} . In figure 5(B), we display a histogram of P_f/P_{max} for all data points in figure 4. For the vast majority of our devices, figure 5(B) shows that $P_f \approx P_{max}$, as anticipated. Because the final resistance R_f is generally a bit larger than $|Z_s|$ (figure 5(A)), we infer that the process tends to stop to the right of the maximum in the inset of figure 5(B).

Relating the junction temperature T to the power P is not straightforward, but it can be stated that T is related to the volume power density p . If we assume for simplicity that only the junction cross section A changes during wire formation, but not its length L , we have $p := P/AL$. Because $R \propto 1/A$ one may also write $p \propto PR$. Hence, in the beginning, when $R \gg |Z_s|$ and $P = V_{in}^2/R$, the power density is constant, even if A increases due to the thermally driven diffusion of Au atoms. This homogenization process can therefore go on at constant temperature until the assumption $R \gg |Z_s|$ is no longer valid. Then, p and hence T will decrease, limiting atomic diffusion. This picture suggests that the homogenization process can proceed further for small $|Z_s|$ as compared to large $|Z_s|$. It therefore becomes understandable why wire-like devices appear for small $|Z_s|$, whereas chain-like ones appear for large $|Z_s|$, consistent with the inset of figure 5(A).

In the previous discussion, electromigration was ignored, since it does not occur for the ac current densities we apply [28]. In fact, electromigration at similar dc current densities leads to gap formation [2, 3, 31], which is the *opposite* effect compared to the new ‘gap-closing’ process that we report here. Interestingly, the series impedance and Joule heating play a similar role in electromigration experiments as in the work presented here [31]. We speculate that repeated gap formation and closing should be possible by using ac and dc voltages, alternately.

4. Conclusions

We demonstrate a simple method to control the formation of metallic nanowires and chains of desired length and diameter. It is based on the dielectrophoretic trapping of nanoparticles. We point out the relevance of two processes: the trapping and the subsequent anchoring of the particles between the electrodes. By choosing a proper series impedance, one can tune the final resistance and appearance of a junction: lower series impedances favour wire formation, whereas higher series impedances result in chains. The nanostructures produced are promising elements in the framework of nanoelectronics. For instance, they can be used to contact nanometre-size building blocks, possibly in combination with

dc electromigration. Using this approach, it may become possible to fine tune nanogaps in electromigration devices, which is of great interest to molecular electronics.

Acknowledgments

We are grateful to M Steinacher for his technical support. SJvdM acknowledges the Netherlands Organisation for Scientific Research, NWO(‘Talent stipendium’). This work was supported by the Swiss National Science Foundation, the Swiss National Center of Competence in Research ‘Nanoscale Science’ and the European Science Foundation through the Eurocore program on Self-Organised Nanostructures (SONS).

References

- [1] Wind S J, Appenzeller J, Martel R, Derycke V and Avouris Ph 2002 Vertical scaling of carbon nanotube field-effect transistors using top gate electrodes *Appl. Phys. Lett.* **80** 3817–9
- [2] Liang W, Shores M P, Bockrath M, Long J R and Park H 2002 Kondo resonance in a single-molecule transistor *Nature* **417** 725–9
- [3] van der Zant H S J *et al* 2006 Molecular three-terminal devices: fabrication and measurements *Faraday Discuss.* **131** 347–56
- [4] Heath J R and Ratner M A 2003 *Phys. Today* **56** 43–9
- [5] Hipps K W 2003 *Science* **294** 536–7
- [6] Subramanian K R V, Saifullah M S M, Tapley E, Kang D-J, Welland M E and Butler M 2004 Direct writing of ZrO_2 on a sub-10 nm scale using an electron beam *Nanotechnology* **15** 158–62
- [7] Liu K, Avouris Ph, Bucchignano J, Martel R and Sun S 2002 Simple fabrication scheme for sub-10 nm electrode gaps using electronbeam lithography *Appl. Phys. Lett.* **80** 865–7
- [8] Steinmann P and Weaver J M R 2005 Nanometer-scale gaps between metallic electrodes fabricated using a statistical alignment technique *Appl. Phys. Lett.* **86** 063104
- [9] Morpurgo A F, Marcus C M and Robinson D B 1999 Controlled fabrication of metallic electrodes with atomic separation *Appl. Phys. Lett.* **74** 2084–6
- [10] Khondaker A S I and Yao Z 2002 *Appl. Phys. Lett.* **81** 4613–5
- [11] Dadosh T, Gordin Y, Krahn R, Khivrich I, Mahalu D, Frydman V, Sperling J, Yacoby A and Bar-Joseph I 2005 Measurement of the conductance of single conjugated molecules *Nature* **436** 677–80
- [12] Long D P, Patterson C H, Moore M H, Seferos D S, Bazan G C and Kushmerick J G 2005 Magnetic directed assembly of molecular junctions *Appl. Phys. Lett.* **86** 153105
- [13] Liao J, Bernard L, Calame M and Schönenberger C 2006 Reversible formation of molecular junctions in two dimensional nanoparticle arrays *Adv. Mater.* **18** 2444–7
- [14] Xu C *et al* 2006 A combined top-down bottom-up approach for introducing nanoparticle networks into nanoelectrode gaps *Nanotechnology* **17** 3333–9
- [15] Pohl H A 1978 *Dielectrophoresis* (Cambridge: Cambridge University Press)
- [16] Jones T B 1995 *Electromechanics of Particles* (Cambridge: Cambridge University Press)
- [17] Morgan H and Green N G 2003 *AC Electrokinetics: colloids and nanoparticles* (Baldock, England: Research Studies Press Ltd.)
- [18] Washizu M, Suzuki S, Kurosawa O, Nishizaka T and Shinoara T 1994 *IEEE Trans. Ind. Appl.* **30** 835–43
- [19] Dewarrat F, Calame M and Schönenberger C 2002 *Single Mol.* **3** 189–93
- [20] Pethig R and Marx G H 1997 *Trends Biotechnol.* **15** 426–32

- [21] Bezryadin A, Dekker C and Schmid G 1997 Electrostatic trapping of single conducting nanoparticles between nanoelectrodes *Appl. Phys. Lett.* **71** 1273–5
- [22] Hermanson K D, Lumsdon S O, Williams J P, Kaler E W and Veley O D 2001 *Science* **294** 1082–6
- [23] Amlani I, Rawlett A M, Nagahara L A and Tsui R K 2002 *Appl. Phys. Lett.* **80** 2761–3
- [24] Kretschmer R and Fritzsche W 2004 Pearl chain formation of nanoparticles in microelectrode gaps by dielectrophoresis *Langmuir* **20** 11797–801
- [25] Lumsdon S O and Scott D M 2005 Assembly of colloidal particles into microwires using an alternating electric field *Langmuir* **21** 4874–80
- [26] Turkevich J, Stevenson P C and Hillier J 1951 *Discuss. Faraday Soc.* **11** 55–75
- [27] Huang S, Tsutsui G, Sakaue H, Shingubara S and Takahagi T 2001 *J. Vac. Sci. Technol. B* **19** 115–20
- [28] Rodbell K P, Castellano A J and Kaufman R I 1998 Ac electromigration (10 mHz–1 MHz) in Al metallization *AIP Conf. Proc.* **418** 212–23
- [29] Durkan C, Schneider M A and Welland M E 1999 Analysis of failure mechanisms in electrically stressed Au nanowires *J. Appl. Phys.* **86** 1280–6
- [30] Lambert M F, Goffman M F, Bourgoin J P and Hesto P 2003 *Nanotechnology* **14** 772–7
- [31] Trouwborst M L, van der Molen S J and van Wees B J 2006 The role of Joule heating in the formation of nanogaps by electromigration *J. Appl. Phys.* **99** 114316
- [32] Tsong T T 1991 Effects of electric field in atomic manipulations *Phys. Rev. B* **44** 13703–10
- [33] Méndez J, Gómez-Herrero J, Pascual J I, Sáenz J J, Soler J M and Baró A M 1996 Diffusion of atoms on Au(111) by the electric field gradient in scanning tunneling microscopy *J. Vac. Sci. Technol. B* **14** 1145–8